Research article

Pantothenate kinase: A promising therapeutic target against pathogenic *Clostridium* species

Soharth Hasnat [a,b,c], M. Nazmul Hoque [b,*], M Murshida Mahbub [c], Tahsin Islam Sakif [d], A.D.A. Shahinuzzaman [e], Tofazzal Islam [a,**]

[a] *Institute of Biotechnology and Genetic Engineering (IBGE), Bangabandhu Sheikh Mujibur Rahman Agricultural University (BSMRAU), Gazipur, 1706, Bangladesh*
[b] *Molecular Biology and Bioinformatics Laboratory (MBBL), Department of Gynecology, Obstetrics and Reproductive Health, BSMRAU, Gazipur, 1706, Bangladesh*
[c] *Department of Genetic Engineering and Biotechnology, East West University, Dhaka, 1212, Bangladesh*
[d] *Lane Department of Computer Science and Electrical Engineering, West Virginia University, Morgantown, WV, WV 26506, USA*
[e] *Pharmaceutical Sciences Research Division, Bangladesh Council of Scientific and Industrial Research (BCSIR), Dhaka, 1205, Bangladesh*

ARTICLE INFO

ABSTRACT

Current treatment of clostridial infections includes broad-spectrum antibiotics and antitoxins, yet antitoxins are ineffective against all *Clostridium* species. Moreover, rising antimicrobial resistance (AMR) threatens treatment effectiveness and public health. This study therefore aimed to discover a common drug target for four pathogenic clostridial species, *Clostridium botulinum*, *C. difficile*, *C. tetani*, and *C. perfringens* through an *in-silico* core genomic approach. Using four reference genomes of *C. botulinum*, *C. difficile*, *C. tetani*, and *C. perfringens*, we identified 1484 core genomic proteins (371/genome) and screened them for potential drug targets. Through a subtractive approach, four core proteins were finally identified as drug targets, represented by type III pantothenate kinase (CoaX) and, selected for further analyses. Interestingly, the CoaX is involved in the phosphorylation of pantothenate (vitamin B5), which is a critical precursor for coenzyme A (CoA) biosynthesis. Investigation of druggability analysis on the identified drug target reinforces CoaX as a promising novel drug target for the selected *Clostridium* species. During the molecular screening of 1201 compounds, a known agonist drug compound (Vibegron) showed strong inhibitory activity against targeted clostridial CoaX. Additionally, we identified tazobactam, a beta-lactamase inhibitor, as effective against the newly proposed target, CoaX. Therefore, identifying CoaX as a single drug target effective against all four clostridial pathogens presents a valuable opportunity to develop a cost-effective treatment for multispecies clostridial infections.

1. Introduction

The *Clostridium* genus comprises Gram-positive, spore-forming anaerobic bacteria, with over 209 species and 5 subspecies [1]. Typically found in soil and gut flora, most Clostridia are harmless. However, four species—*C. tetani, C. difficile, C. botulinum*, and *C. perfringens*—produce harmful exotoxins [2], collectively infecting over 4.5 million people annually worldwide [3–5]. In 2015,

---

* Corresponding author.
** Corresponding author.
E-mail addresses: nazmul90@bsmrau.edu.bd (M.N. Hoque), tofazzalislam@bsmrau.edu.bd (T. Islam).

C. tetani alone caused 56,000 global deaths [3,6], while *C. difficile* is responsible for over 29,000 deaths annually in the United States of America [7]. Untreated infections from these pathogens can lead to severe complications and increased mortality risk. *C. tetani*, a notable exotoxin-producing species, is responsible for tetanus, typically entering the host through wounds or cracked skin [8]. Treatment for tetanus often involves broad-spectrum antibiotics, as no specific medications are available [9]. Similarly, *C. difficile* is notorious for causing nosocomial antibiotic-associated diarrhea, [10]. The treatment and management of *C. difficile* infections vary based on disease severity. Currently, available antibiotic treatments are predominantly broad-spectrum, including vancomycin, tazobactam, and metronidazole (Gerding et al., 2008; Kukla et al., 2020). Various forms of botulism, caused by botulinum neurotoxins (BoNTs) from *C. botulinum*, result in distinct types like wound botulism and foodborne botulism [11]. While antibiotics are not typically the primary treatment for botulism, they may be administered to prevent bacterial proliferation in cases of wound botulism. However, the challenge with antibiotic use lies in the risk of promoting antimicrobial resistance (AMR), necessitating careful management to minimize this risk. Commonly used antibiotics for botulism treatment include broad-spectrum options such as tetracycline, tazobactam, penicillin, rifampin, metronidazole, erythromycin, and chloramphenicol (Khademi & Sahebkar, 2019; Kundrapu et al., 2016). *C. perfringens,* transmitted through food, causes gas gangrene, a highly lethal soft tissue infection [12]. While the incidence of
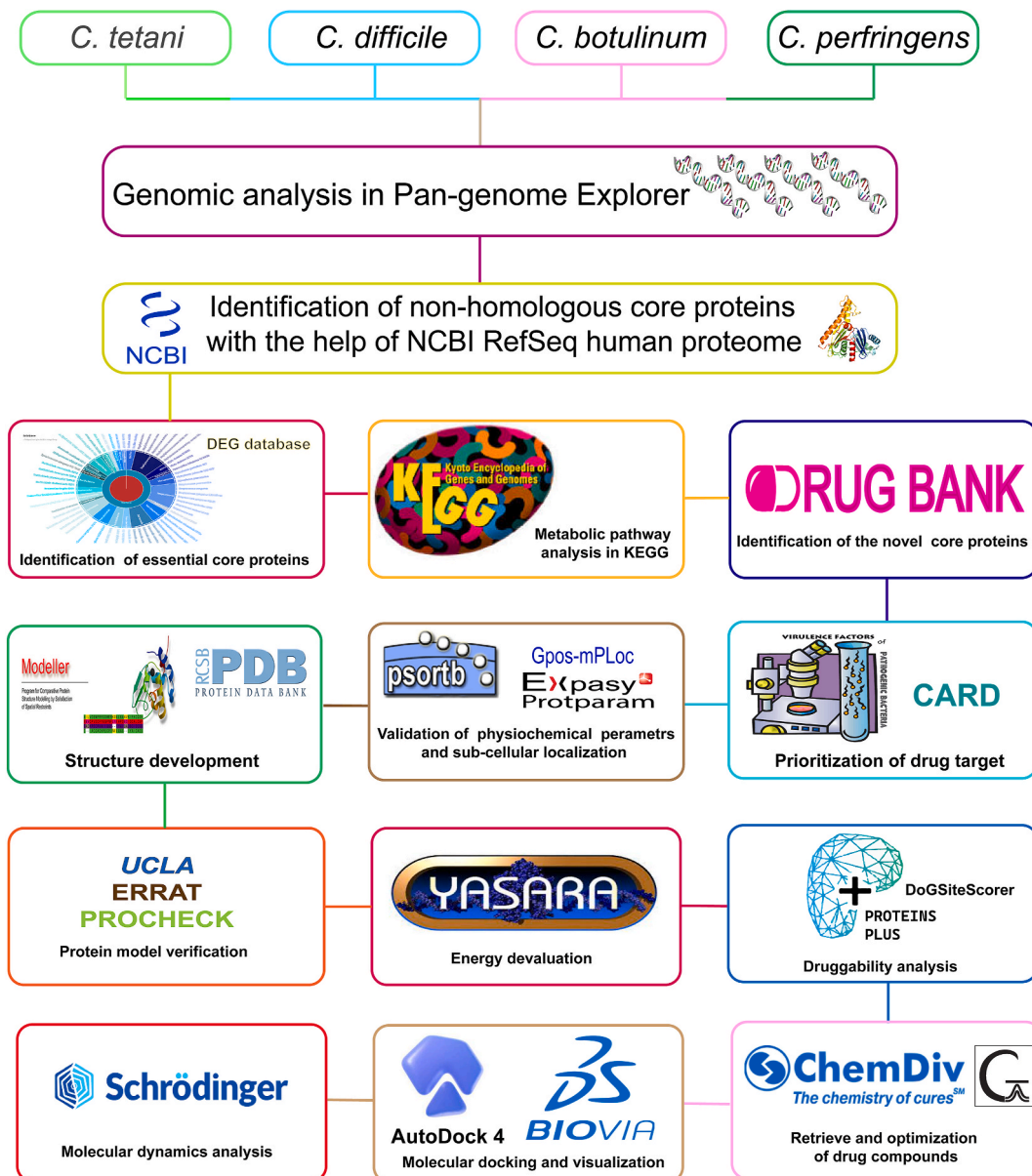
Fig. 1. Overview of core genomic approach identifying drug targets of the pathogenic bacterial species and proposing potential drug candidates using cutting-edge tools.

C. perfringens infections may not be as prevalent as those caused by other Clostridium species, untreated infections carry a 100 % fatality rate [12], no alternative are available except broad spectrum antibiotics [13,14]. Treatment management for pathogenic closteridial species heavily relay on broad spectrum anibiotics and there is no specific medication are available. Although the pathogenicity of different Clostridium genera is caused by various types of toxins [15], so it is important to use drugs or alternative therapies with bactericidal power that do not lyse the vegetative cells to reduce the amount of toxin produced. To avoid this issue, no membrane proteins were selected as drug targets. Instead, this study identified the cytoplasmic CoaX protein, present in four pathogenic species of *Clostridium*, as a potential drug target. Bacterial CoaX catalyzes the first and rate-limiting step in the biosynthesis of coenzyme A (CoA), converting pantothenate (vitamin B5) into 4′-phosphopantothenate using ATP as a phosphate donor [16,17]. This pathway is a promising source of novel drug targets because CoA is essential as a cofactor and for regulating key metabolic enzymes in various cellular processes, including lipid biosynthesis and catabolism [17,18]. Additionally, the coaX gene is crucial for bacterial growth both *in vitro* and *in vivo* [19].

However, advanced *in silico* drug development strategies offer great opportunity for identifying specific drug targets. Our genome analysis reveals essential proteins unique to pathogenic bacteria, presenting attractive targets for designing new antibiotics. Molecular dynamics simulations play a crucial role in validating the drug discovery process, offering promising avenues for combatting *Clostridium* infections. Therefore, this study aimed to discover a common drug target for four pathogenic *Clostridium* species, utilizing diverse databases and computational tools to identify inhibitory compounds.

2. Methods and materials

2.1. Collection of core genomic proteins

Four reference genomes were obtained from the National Center for Biotechnology Information (NCBI), representing *C. botulinum* (accession number: GCF_000007625.1), C. difficile (accession number: GCF_020138775.1), C. tetani (accession number: GCF_018885085.1), and C. perfringens (accession number: GCF_000063585.1). The Pan-genomic Explorer (PGE), a web server for pan-genomic studies [20], was employed to identify the core genomic proteins present among the reference genomes (Fig. 1). PGE providing various genomic analyses and reports, giving intuitive views that enable a better understanding of bacterial genomes [20]. Moreover PGE's prokaryotic genome annotation pipeline arranges genes through Hierarchical Clustering(presence/absence variation matrix) and uses the hotmap.js javascript library for data visualization [20]. Various criteria were followed to identify core proteins from the total proteomes, including their presence in all chosen proteomes, a minimum of 50 % sequence similarities, consistent functional annotation, and absence of redundancy. The PGE program ran with the PanACoTA pipeline [21] and the threshold percentage was set at 50 for identifying core protein. The program pointed three categories of clusters: core, dispensable, and strain-specific genes, alongside the distribution of core and accessory genomes. In this contemporary core genomic investigation, only core proteins (present in four organisms) were taken for subsequent study.

2.2. Identification of non-homologous clusters

In the subsequent stage of analysis, non-homologous core proteins, which lack similarities with host organisms, were identified by running the Basic Local Alignment Search Tool for proteins (BLASTp) against the Homo sapiens proteome (Grch38) available on NCBI [22,23]. Subsequently, the human proteome database was created to identify core proteins that share similarities with the host proteome. In this investigation, all BLASTp analysis was performed with an e-value cutoff score of 10^{-4}, sequence identity 35 %, bit score 100, and others as default [24–26]. Here the cutoff score of 10^{-4} suggests that the alignment is very unlikely to have occurred by chance (or 1 in 10,000), indicating a potentially meaningful biological relationship between the sequences [27]. The bit score 100 indicates a high-quality alignment between the query sequence and the database sequence [27]. Besdies sequence identity ≥30 increases the chances of functional similarities between query and target proteins [28,29]. The BLASTp generated results, i.e., 'Hits Found' (homologous sequences amongst pathogen and the host) were excluded, and 'No-Hits Found' (Non-homologous sequences to human proteome) were taken for further investigation to avoid off-targeting.

2.3. Identification of essential core proteins

Essential proteins play a significant role in cellular metabolism and are also required for the survival and growth of any organism [30]. Essential genes for prokaryotes were collected from the Database of Essential Genes (DEG), a curated repository encompassing essential genes for prokaryotes, eukaryotes, and archaea [31]. DEG constitutes the database based on experimental validation of genes that are minimally required for a living cell and are likely to be common to all cells [31]. Once more, BLASTp was operated alongside the identified non-homologous core proteins and the bacterial essential proteins with an e-value cutoff score of 10^{-4}, sequence identity 35 %, bit score 100, and others as default [25,26]. A protein was selected for further analysis only if identified as a core protein and exhibited similarities with essential proteins. Proteins that exhibited similarities with DEG proteins were considered essential for *Clostridium* species.

2.4. Metabolic pathway analysis

The KEGG Automatic Annotation Server (KASS) was employed to identify core proteins with complete metabolic pathway

information [32]. Initially, the identified essential core proteins were used as queries in the KASS server. Subsequently, a job request for pathway information in KASS was submitted using the prokaryotic representative gene set. Potential drug targets were then chosen from the KEGG Orthology (KO) list, considering the availability of complete metabolic pathway information. Additional job requests were placed with the consistent query sequences in KASS, which were made by selecting representative gene sets for eukaryotes to exclude the proteins that share similarities with human metabolic pathways. In the final step, proteins were only chosen for the subsequent analysis when each protein of a core shared the same KO number.

2.5. Identification and prioritization of novel drug targets

To identify and prioritize novel drug targets, we employed several filtration steps. Initially, core proteins with complete pathways were aligned with the previously identified drug target proteins. The earlier identified target proteins were obtained from the Drug Bank repository [33]. Core proteins were found to have no similarities with the previously identified drug target proteins, indicating they might represent potential novel targets. Likewise, the novel targets were aligned with the Comprehensive Antibiotic Resistance Database (CARD) [34]. Proteins that manifested no similarities with CARD proteins were picked up to run the final BLASTp alignment with the Virulence Factors Database (VFDB) setting the e-value cutoff score of 10^{-4}, sequence identity 35 %, bit score 100, and others as default to substantiate the proteins having virulence features [35]. The virulence of bacterial pathogens quantifies their pathogenicity. VFDB defines virulence factors as products of virulence genes that allow microorganisms to establish themselves within a host and enhance their ability to cause disease [35]. The relevance of these factors to Clostridium proteins has revealed the presence of virulence factors in Clostridium species.

2.6. Potentiality analysis of the drug targets

The previous strategies for identifying drug targets were further carefully reviewed to confirm the final selection of drug targets thoroughly [36,37]. In this analysis, the first step involved studying two essential parameters: subcellular localization and physicochemical properties of the identified core proteins. We applied PSORTb version 3.0.3 and Gpos-mPLoc to analyze the sub-cellular localization of the identified core protein sequences, as these tools are commonly used for sub-cellular localization of proteins [38, 39]. PSORTb was configured for a bacterial organism with a Gram-positive stain option and set to generate output in the normal format. The output of PSORTb predictions was interpreted based on the subcellular localization score and the final determination of the protein's localization such as cytoplasm, cytoplasmic membrane, inner membrane, outer membrane and periplasmic membrane, extracellular region, and undetermined [40]. Proteins in various subcellular compartments perform essential functions for cell viability. Targeting these proteins can disrupt critical pathways crucial for pathogen survival or disease progression [41]. Furthermore, the ProtParam toolkit was unified to become competent in the physicochemical properties of core proteins, specifically the molecular weight, average hydropathicity (GRAVY) value, isoelectric point (PI), and aliphatic index [42]. The core proteins with low molecular weight (>100 kDa) were deemed as an essential feature of an adequate drug target on account of the higher accessibility of lower molecular weight proteins [43]. The other three properties such as GRAVY, PI and aliphatic index were also investigated to justify the novel core proteins as proficient targets.

2.7. Structure curation and validation

Due to the unavailability of experimentally confirmed structures for our top core targets, we employed the MODELLER program to construct the structures of the selected core proteins based on experimentally confirmed protein that has around 60 % sequence identity and 98 % area coverage with selected core proteins. MODELLER is a computational tool used for homology or comparative modeling of protein three-dimensional structures, predicting a protein's structure based on its alignment with known protein structures. In this investigation, MODELLER aided in building the 3D structure of the desired protein [44], ultimately facilitating further research on the targeted protein. Subsequently, validation steps were carried out to ensure the quality of model structures. In this investigation, the quality of the model structures was assessed using ERRAT and PROCHECK. ERRAT was utilized to assess the protein structures and evaluate the patterns of nonbonded atomic interactions and the generally accepted range is > 50 for a high quality model [45,46]. Finally, PROCHECK was employed to examine the structural stereochemical quality by analyzing the residue-by-residue and overall geometry of the model structure [47].

2.8. Druggability analysis of the pockets

Prior to conducting the druggability analysis, we carried out energy minimization of the model protein's tertiary structure using the YASARA force field [48]. YASARA force field can calculate force field energies of a protein individually (atom, residue, molecule, object) to locate regions of interest. YASARA uses eigenvector analysis to calculate angles and dihedrals between groups of atoms like helices or planar sidechains which is suitable for studying biomolecules [49]. Energy depreciation was required to confirm the proper molecular arrangement that turned the structures energetically favorable [50]. Each energetically favorable structure returned with the minimal energy value and Z score, and visualize them in YASARA view. The subsequent values of Z were considered ≥ -3 bad, ≤ -2 satisfactory, and ≤ -1 good (the Z score expressed the standard deviations from the standard). The drug-friendliness of the target core proteins was assessed using DoGSiteScorer, which identified potential drug-binding pockets. DoGSiteScorer is an automated algorithm for predicting pockets and druggability, utilizing a difference of Gaussian filter to detect possible binding pockets [51]. The

range of druggability scores from 0 to 1 was also documented, and higher scores are assumed to be more drug-friendly pockets [51]. In the final step, a reference protein (PDB ID: 2H3G) with the highest sequence similarity to the selected core protiens, including known active and binding sites [52], was obtained from the Protein Data Bank (PDB). This step was useful to spot the position of essential residues in final core proteins with the help of reference protein by UCSF Chimera [53].

2.9. Compound collection and optimization

A total of 1201 inhibitor compounds were downloaded from the natural product-based library of ChemDiv (https://www.chemdiv.com/). As a first assignment, we examined Lipinski's rule of five using MarvinSketch 23.5 [54] to ensure each compound adheres to all of the rules. MarvinSketch was employed to convert all molecules from SDF to Mol format. Subsequently, we conducted initial optimization of each molecule using Avogadro and saved them in PDB format [55]. Finally, the geometry of each drug candidate was optimized in Gaussian using the universal force field method [56]. The workflow for running the Gaussian program is available in the S1 file.

2.10. Molecular screening

Each core protein underwent preprocessing prior to molecular screening, involving the removal of water molecules using Auto-DockTools followed by the addition of hydrogens and charges to each protein's structure [57–59]. Next, the proteins and ligands in PDB format were successively converted into pdbqt format using AutoDockTools and Open Babel [59,60]. Screening analysis was conducted using AutoDock Vina. The grid box was constructed within the active site of the core proteins, with dimensions x = 29.2221, y = 40.99, and z = 34.76, and a grid point spacing of >25 Å. The coordinates for the grid center were x = 36.4725, y = 50.1742, and z = 3.86 [61,62]. The grid box position was kept constant for each selected core protein to ensure a homogenous screening environment [61,62]. AutoDock Vina was executed through a batch script, which sequentially executed commands to operate the software [63]. Subsequently, multiple models (typically 1 to 9) were generated for each receptor-ligand interaction during docking, but the model that showed the highest binding free energy with the lowest RMSD score was considered as best [64]. The receptor-ligand interaction providing the highest free energy for each returned ligand model was analyzed using Discovery Studio Visualizer [65]. Our evaluation focused on the surface of the hydrogen bond donor and acceptor as the primary feature in receptor-ligand interaction. Finally, to gain a deeper understanding of the interactions, each interaction and its type between ligands and selected proteins were examined closely.

2.11. Molecular dynamic simulation studies

The initial molecular screening offered insights into protein-ligand interactions, leading to further assessment through molecular dynamics. Forty protein-ligand complexes, comprising nine compounds and one reference compound against each protein, were selected based on screening results. In the absence of *Clostridium*-specific drugs, the broad-spectrum antibiotic tazobactam was chosen for comparison as a reference. Additionally, four simulations were conducted on the final core proteins (CoaX) to assess their stability, and a single molecular dynamics simulation was performed to monitor changes in the beta-3 adrenergic receptor protein following binding of SN1382 (Vibegron), an agonist drug compound that targets the beta-3 adrenergic receptor. Each 200 ns simulation provided detailed atomic insights into the protein and protein-ligand complexes over time [66]. Molecular dynamics simulations (MDS) were conducted using the Desmond package in Schrödinger suite v2023-4, commonly employed to analyze alterations within the solvent system surrounding the protein-ligand complex [15]. The preparation step for running a simulation was set in motion by protein preparation, and incorporating steps were preprocessing refinement and geometry optimization. Subsequently, the system builder was utilized to prepare the protein-ligand complex. The SPC water model was chosen, configured in an orthorhombic shape after volume minimization, with 10 Å × 10 Å × 10 Å periodic boundary conditions applied along the x, y, and z axes of the protein-ligand complex. Additionally, Na + ions were added to neutralize the system, excluding ion and salt placement within 20 Å to maintain neutrality. The OPLS2005 force field was used to minimize the complex's energy through heating and equilibrium processes before starting the production run of MD simulations [67]. Each complex underwent energy minimization using the steepest descent method, followed by heating from 0 to 300 K. The system was then equilibrated with a time step of 200 ps for 1000 steps. The final production run was conducted for 200 ns with a time step of 200 ps, maintaining a temperature of 300 K, a energy value 1.2, and a pressure of 1.01325 atm, using the Nose-Hoover method within an NPT ensemble [68]. Running on an NVIDIA GeForce RTX 4070 GPU, each 200 ns simulation took approximately 8 h. Frames were collected and analyzed using a simulation interaction diagram to examine trajectories and fluctuations.

2.12. Binding free energy analysis

Thermal MM-GBSA (Molecular Mechanics Generalized Born Surface Area), is commonly employed to estimate the binding free energy between molecules, such as protein-ligand complexes [69]. To calculate MM-GBSA from the completed 200 ns trajectories, each trajectory was divided into ten frame snapshots, and the free energy across the 200 ns simulation time was estimated. Once the Desmond MD trajectory was divided into ten frame snapshots, the ligand and receptor were isolated for MM-GBSA calculation for each of the snapshots.

3. Results

3.1. Collection of core genomic protein

This *in silico* investigation aimed to utilize computational methods to pinpoint promising drug targets within pathogenic clostridium species, offering an economically viable therapeutic approach for managing multispecies clostridial infections. The outcome of the PGE analysis revealed that a collective of 1484 proteins (with 371 core proteins per genome) were identified as core genomic proteins across the four reference clostridium genomes. The coverage of the detected core genomic proteins was 4.2 %, considering the size of the pan-genomes of the chosen species of the pathogenic *Clostridium*. Analysis of the whole genomes of the four species in PGE pinpointed that 80.3 % of proteins in *C. botulinum, C. difficile, C. tetani, and C. perfringens* were strain-specific, and the remaining 15.5 % were dispensable (Fig. S1).

3.2. Identification of non-homologous and essential core proteins

To identify the non-homologous core proteins, BLASTp analysis against the human proteome were performed against the host (*Homo sapiens*) proteome. After filtering the BLASTp results, a total of 632 core proteins (comprising 158 core proteins per genome) exhibited similarity with human proteins, and these proteins were excluded from downstream analysis due to potential cross-reactivity and undesired toxicity in the host. In a subsequent alignment analysis, 26,619 essential prokaryotic proteins aligned with identified 632 non-homologous proteins to the host. Indeed, 538 core proteins (comprising 137 proteins per genome) were discovered to exhibit similarities with prokaryotic essential proteins, suggesting their significance for the selected organisms.

3.3. Metabolic pathway analysis

The metabolic pathway analysis conducted with KEGG unveiled that out of 538 core proteins, 344 proteins (comprising 86 core proteins per genome) have had complete metabolic pathways. The remaining 194 core proteins were excluded since no unique accession for the KEGG pathway map was found to assign against them. However, out of these core proteins (n = 344), only 156 (39 proteins per genome) possessed complete pathway information, and were included in the subsequent analysis as potential drug targets. Additionally, one protein from each of the reference genome shared metabolic pathways with the host, leading to their exclusion to ensure that the selected drug targets bore no resemblance to human metabolic pathways.

3.4. Identification and prioritization of novel targets

For the novel drug target prioritization, 5346 previously identified drug targets were taken from the Drug Bank database to align against the proteins (n = 156) with complete metabolic pathways. Subsequent alignment uncovered that 44 core proteins (comprising 11 proteins per genome) showed no similarities with previously identified drug targets. Consequently, they were considered as novel candidates for drug targeting. Further refinement involved aligning these 44 proteins against 317,119 proteins available in the CARD database. Alignment analysis against CARD proteins revealed that only eight core proteins (two proteins per genome) exhibited similarities with antibiotic-resistance proteins, and were subsequently excluded from further analysis. In the last filtration step, thirteen proteins demonstrated similarity with the VDFD (Virulence Factors Database) proteins. Eventually, only eight core proteins comprising two proteins per genome of *Clostridium* were selected as novel drug targets. The remaining core proteins were excluded because they did not share similarities with VDFD proteins. Finally, these eight core proteins were found to be represented by SecA and CoaX (in each of four *Clostridium* species) were identified and selected for further analyses.

3.5. Potentiality of the drug targets

To identify a potential drug target for pathogens like *Clostridium* subcellular localization was the first concern when considering any drug target as a potential candidate. The subcellular localization tools PSORTb and Gpos-mPLoc have identified the final set of eight core proteins, with four pertaining to SecA (Group 1) and four to CoaX (Group 2) proteins, all residing within the cytoplasm. In

Table 1
Physiochemical properties and subcellular localization of SecA and CoaX proteins.

Core proteins	Organism	Protein name	GRAVY score	Molecular weight (kDa)	PI value	Aliphatic index	Subcellular localization
Group 1	*C. botulinum*	SecAb	−0.566	95.6	5.33	86.6	Cytoplasm
	C. difficile	SecAd	−0.507	101.57	5.74	87.16	Cytoplasm
	C. tetani	SecAt	−0.574	96.7	5.27	87.93	Cytoplasm
	C. perfringens	SecAp	−0.557	95.58	5.49	84.24	Cytoplasm
Group 2	*C. botulinum*	CoaXb	0.138	28.3	6	110.31	Cytoplasm
	C. difficile	CoaXd	0.103	27.94	5.6	106.95	Cytoplasm
	C. tetani	CoaXt	0.089	28.6	5.34	108.24	Cytoplasm
	C. perfringens	CoaXp	−0.072	28.8	6.36	101.97	Cytoplasm

(Here, SecA and CoaX are protein names, b = *C. botulinum,* d = *C. difficile,* t = *C. tetani,* and p = *C. perfringens*).

PSORTb, the likelihood scores for locating the proteins in the cytoplasm were more noteworthy than in any other subcellular location. The quantitative values for physiochemical parameters and molecular weight of core proteins determined by ProtParam definite the potentiality of the discovered core proteins, as illustrated in Table 1. An important parameter, the molecular weight of the proteins from each of the four strains, was tight to each other. Remarkably, the molecular weight of the Group 2 protein (CoaX) was below 30 kDa (Table 1). Anticipated GRAVY scores of the Group 2 were positive; though the only oddity was CoaX from *C. perfringens*. Positive Gravy scores mean that the protein of the Group 2 is more hydrophobic than that of the Group 1 (Table 1). Another crucial parameter, the isoelectric point (pI), exhibited values ranging from 5.27 to 6.36 across eight proteins. The final parameter, the Aliphatic index value, exceeded 100 for the type III pantothenate kinase (CoaX) proteins (Table 1). Taking into account all parameters, CoaX emerged as a preferred and promising drug target for *Clostridium* species.

3.6. Structure curation and validation of the drug target (CoaX)

The structures were constructed for the best potential target type III CoaX. An experimentally determined structure (PDB ID 2H3G) was brought as a template for ensembling the structure for target core proteins. CoaX from *Bacillus anthracis* shares 59.53 %, 59.06 %, 60.08 %, and 61.0 % similarities with *C. botulinum, C. difficile, C. tetani*, and *C. perfringens*, respectively. Subsequently, the anticipated overall quality scores by ERRAT for model structures for CoaX proteins were 94.58, 95.41, 91.18, and 92.80 (Fig. S2). The successive stage of quality assurance analysis, employing PROCHECK, demonstrated that more than 90 % of the residues in four proteins were present in the acceptable regions (Fig. S2). Only a small percentage of residues (4.9 %–6.6 %) were found to fall in the additional allowed regions and less than 1 % of the total residues were found in both disallowed and generously allowed regions (Fig. S2).

3.7. Energy minimization and druggability

We performed energy minimization to lower the Gibbs free energy of model protein structures. The YASARA force field enabled us to devalue the energy state by around 70,000 kj/mol energy for each protein (Table 2). Additionally, the value of Z scores also improved as the force field devalued Gibbs's free energy. All negative Z scores (negative score means deviations of the structure quality considering the energy state) maximized into positive values, which means structure quality improved after the minimization process (Table 2). Following the improvement of the energy state, the analysis of druggability was conducted using DoGSiteScorer. We found ten druggable pockets for each core protein. Consequently, the binding sites with the maximum druggability score were deemed equally as the best optimal druggable pocket for the target proteins. A common drug binding area was found among the four drug target proteins (Fig. 2A). The scores for the best druggable pockets for the targeted core proteins were around 0.8 out of 1, indicating excellent affinity for drug binding to the pocket region (Table 2). A pocket with the highest volume (Å^3), surface area (Å^2), and the higher druggability score was supposed to be a more druggable pocket for the drug molecules. The volume and surface of the best druggable pockets ranged from 985 to 1220 Å^3 and 1373–1613 Å^2 (Table 2). After identifying the pockets, the locality of the active sites and binding site residues were determined with the help of reference structure (PDB ID 2H3G). The surface area created by active and binding site residues was exactly similar to the surface of the best druggable pocket areas (Fig. 2A and B). Likewise, all the active site and binding site residues of four core proteins situated within the pocket regions are positioned nearly identically (Fig. 2C).

3.8. Molecular screening of ligands against the drug target

In molecular screening, 1201 compounds were taken randomly from natural product-based library of ChemDiv and a known irreversible inhibitor tazobactam (reference compound) were screened against each of the desirable core proteins. This large-scale screening showed nine compounds from the total compounds had the highest binding affinity and stable receptor ligand interaction, which released more than 8.0 kcal/mol when forming complexes with each core protein (Table 3). The compounds exhibiting significant free binding energy with CoxA proteins were investigated further using Discovery Studio Visualizer to evaluate the interaction types, their strength, and interacting amino acids. Type III CoaX acquired the following ATP-binding amino acids: Asp6, Val7, Ans9, Thr10, Asn11, Val13, and Thr132 (Fig. 2C). Moreover, four amino acids, namely Gly-Ala-Asp-Arg, fall between 107 and 110 and are involved in substrate binding (Fig. 2C). The other two crucial amino acids, Asp129, act as a K^+ binding site and Thr132 is conserved for Phosphate2 (Fig. 2C). In our findings, receptor-ligand interactions were found with the aforesaid active and binding site residues for each best-docked ligand, which expressed the inhibitory capabilities of the top free energy-releasing ligands (Fig. 3). The receptor-ligand interactions were mediated by various intermolecular forces, especially electrostatic interactions, hydrogen bonds (H-bond), van der Waals forces, and hydrophobic interactions (Fig. 3). Based on a comprehensive analysis of protein-ligand binding

Table 2
Values of energy minimization and druggability of drug-binding pockets of CoaX proteins.

Protein Id	Energy level (kj/mol) before minimization	Energy level (kj/mol) after minimization	Z score before energy minimization	Z score after energy minimization	Pockets volume Å^3	Pockets Surface Å^2	Druggability score
coaXt2	−204058	−281084	−0.97	0.11	985.98	1399.12	0.8
coaXd2	−200150	−278743.9	−0.96	0.34	1016	1414.77	0.79
coaXb2	−207259	−276576	−0.61	0.2	985.41	1373.92	0.8
coaXp2	−209962	−282316	−0.8	0.2	1219.97	1613.16	0.8
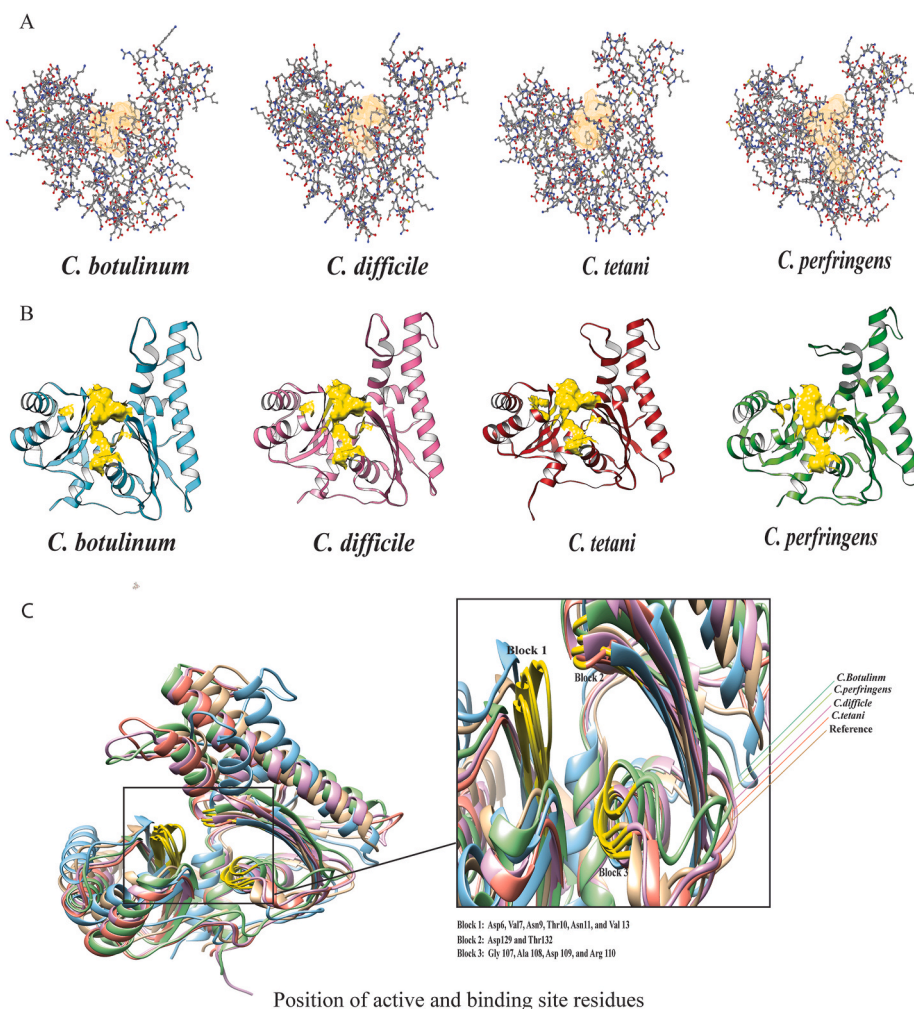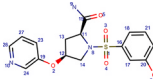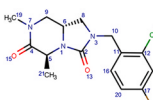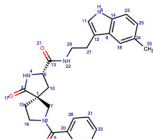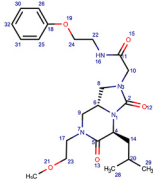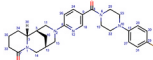
Fig. 2. Study the robustness of drug-binding pockets. (A). Representation of best druggable pockets for the CoaX proteins of the selected Clostridium detected by DoGSiteScorer. (B). Representation of the surface area in the drug binding pockets created by active residues. (C). Identificati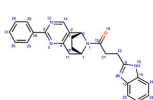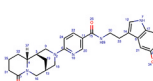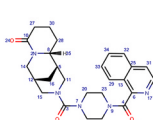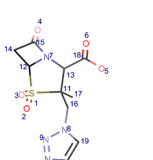on of the position of active and binding residues with the help of the reference structure and comparison with drug binding pockets.

affinity, and their interactions with active and binding site residues, three compounds such as SN1382, SN1414 and SN2936 were thought to be the most satisfactory among the nine complexes. Compound SN1382 (Vibegron) established hydrogen bonds with the oxygen and hydroxy groups of the active and binding site residues Asn9, Asn11, Asp109, Arg110, and Asp129 of CoaX proteins. (Fig. 3). H-bonding was also observed in the two other top-docked receptor-ligand complexes; however, they were not as robust as the SN1382-CoaX complexes (Fig. 3). The most substantial H-bond donor and acceptor created crucial surface regions in the druggable pockets, and their comparisons recommended that SN1382 formed a more favorable surface compared to the other two compounds (Fig. 3A - C). The top three docked compounds also exhibited several interactions, including Pi-Donor, Pi-Anion, Alkyl, and Pi-Alkyl interactions, with neighboring amino acids within the ligand binding pockets. However, compound SN1382 demonstrated interaction with crucial amino acids, though variations were observed in pharmacophore properties corresponding to CoaX proteins of selected *Clostridium* (Fig. 3A). Notably, ligands interact with almost identical residues across four proteins, albeit via distinct functional and side chain groups. For example, ligand atom O19 establishes H-bonds with the side chains of Asp109 and Arg110 residues within the CoaX protein of *C. botulinum* (CoaXb). Conversely, ligand atom N4 displayed H-bonding with Asp109 residues of CoaX protein of *C. difficile* (CoaXd). Moreover, the non-specificity of ligand atoms to amino acids was also observed in CoaX ptotein of *C. tetani* (CoaXt) and *C. perfringens* (CoaXp) proteins (Fig. 3A–Table 3). Similar facts were also found in the receptor-ligand interaction of SN1414-CoaXb and SN2936-CoaXp (Fig. 3B and C). Simultaneously, the molecular screening of broad-spectrum antibiotic tazobactam was studied, releasing less free binding energies as it interacted with targeted CoaX proteins (Table 3). The aforementioned certainties were also observed with the reference drug compound tazobactam (Fig. S3).

Table 3

Nine compounds are presented with the details of Lipinski's rules and the released free energy during molecular screening.

Compound Id	Structure	H bond acceptor	H bond donor	logP	Molecular Weight (Daltons)	Free energy release during screening (kcal/mol)			
						C. botulinum	*C. difficile*	*C. tetani*	*C. perfringens*
SN145 (CID: 132333685)		9	02	2.51	435	−9.3	−9.4	−9.3	−9
SN154 (CID: 110199111)		9	2	2.07	405	−8	−7.8	−9	−7.8
SN1155 (CID: 137904779)		5	0	2.1	325	−9.4	−10.3	−10	−9.6
SN1382 (CID: 137908674)		7	03	2.72	444	−10.5	−10.2	−10	−9.6
SN1414 (CID: 137892533)		9	01	2.52	446	−10.2	−10.4	−10.1	−10.2
SN1818 (CID: 110195418)		7	0	2.28	477	−9.7	−9.7	−9.8	−9.6
SN2041 (CID: 110196734)		6	1	3.44	409	−9.3	−10.2	−9.7	−9.8
SN2936 (CID: 110195404)		8	2	2.1	487	−10.5	−10.3	−10.3	−10.2
SN2943 (CID: 110195624)		8	0	2.57	461	−8.9	−9.1	−9.1	−9
Tazobactam (CID: 123630)		7	1	1.40	300	−7.9	−8.5	−7.5	−7.7

A

CoaXb

CoaXd

CoaXt

CoaXp

Compound: SN1382

B

CoaXb

CoaXd

CoaXt

CoaXp

Compound: SN1414

C

CoaXb

CoaXd

CoaXt

CoaXp

Compound: SN2936

CoaX is protein name, b = *C. botulinum*, d = *C. difficile*, t = *C. tetani*, and p = *C. perfringens*

(caption on next page)

Fig. 3. Donor-acceptor interaction on account of H-bond created heterogeneous surface regions in ligands and receptor proteins (CoaX) complex. Each compound demonstrated diverse chemical associations with different CoaX proteins. (A). Compound SN1382 (Vibegron) participated in hydrogen bonding (H-bonding) as a donor and acceptor with Coax proteins of each selected species of *Clostridium*. Various types of interactions and their differences were also observed. (B). Representation of the Donor-acceptor surface regions and various types of chemical affinities generated from the interaction of SN1414 with receptor proteins. (C). SN2936 also evoked heterogeneous donor-acceptor surface areas and chemical associations in receptor-ligand complexes.

3.9. Molecular dynamics simulation (MDS)

Molecular screening studies showed primary interactions between the receptor-ligand complexes. For an insight understanding, 40 simulations were performed to assess the discrepancy between the best receptor-ligand complexes. MDS studies displayed the stability of each protein-inhibitor complex, which suggested Vibegron (SN1382) as the finest inhibitory compound against identified CoaX proteins among the nine best-screened compounds.

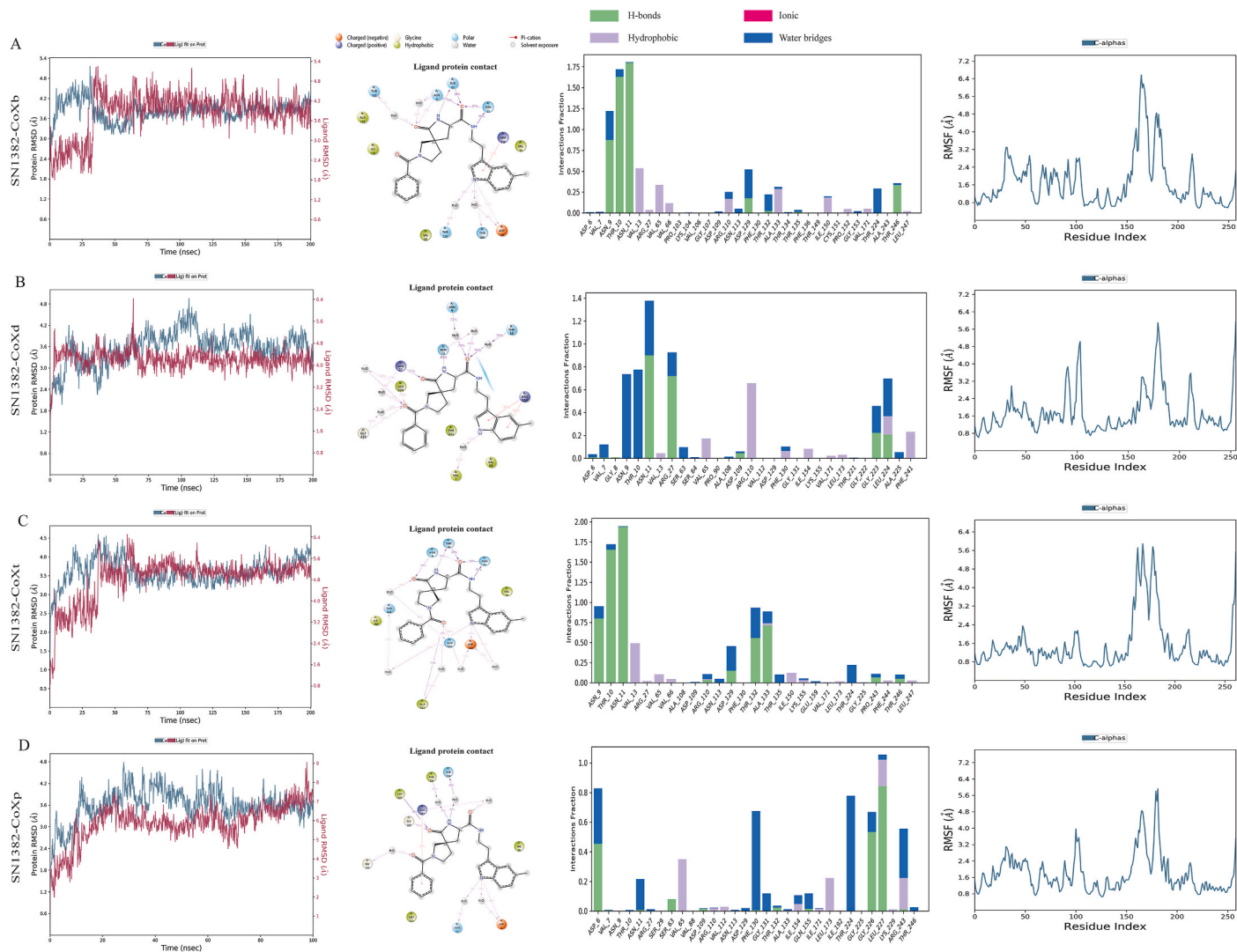#### 3.9.1. Trajectory analysis for Vibegron (SN1382)

Analysis of the snapshots of MDS revealed that active and binding site residue retained solid interaction consistently throughout the 200 ns trajectory. The protein-ligand contact and interaction fractions were significantly robust for the first three complexes depicted in Fig. 4. Over the course of the 200 ns trajectory, the SN1382 exhibited enduring and persistent interactions with key ATP binding residues of CoaXb, CoaXd, and CoaXt proteins through the N4, O17, O21, and N22 atoms presented in Fig. 4A – C and accompanying animations (File. S2A – S2C). However, an anomaly was observed in the SN1382-CoaXp complex on account of a small fraction of the interactions detected with crucial amino acids (Fig. 4D and File S2D). The root mean square deviation (RMSD) value for each CoX-SN1382 complex fell within the range of 1–5 Å, except for the SN1382-CoaXp complex, which displayed broader fluctuations. Specifically, the RMSD value for the CoaXb-SN1382 complex relative to its initial position surged to 4.98 Å within the first 30 ns, then decreased to approximately 4 Å by 150 ns, after which the system equilibrated for the remainder of the trajectory (Fig. 4A). Over the duration, ligand atoms O17, O21, and N22 consistently exhibited heightened affinities toward ASN9, THR10, and ASN11 residues (Fig. 4A and File S2A). The root mean square fluctuations (RMSF) value corresponding to the ligand was stable, especially in the regions where ligand atoms interact with higher affinities (Fig. 4A). In the subsequent analysis, the CoaXb-SN1382 complex demonstrated fluctuations ranging from 1.8 Å to approximately 5 Å before reducing to 4 Å towards the end of the trajectory. This complex notably displayed a pronounced polar and charged affinity, driven by the interactions of O17, O21, N4, and N17 atoms with the ASN9, THR10, and ASN11 residues (File S2B). Additionally, the RMSF values for these residues engaged with the ligand were consistently below 3 Å (Fig. 4B). In the third complex, the trajectory of CoaXt-SN1382 initially ascended to 5.3 Å over the initial 65 ns period relative to its starting position before gradually declining to approximately 4.8 Å (Fig. 4C). Similar to the interactions observed previously, the O17, O21, and N22 atoms of SN1382 demonstrated robust affinities with ASN9, THR10, and ASN11 (File S2C). Regarding CoaXp, it exhibited the highest fluctuations compared to the previous three complexes throughout the simulation trajectory, surpassing 5 Å. Strong hydrophobic and water bridge interactions were observed, particularly between O17—ASP6, N4—THR224, and N4—LEU227 (Fig. 4D and File S2D).

3.9.2. Trajectory analysis for CoaX protein

The 200 ns simulations were conducted focusing on elucidating the detailed stability of each amino acid residue of CoaX proteins. Understanding the stability of residual position was crucial as the protein structures were constructed using homology modeling techniques. Throughout the simulation, the RMSD values of the CoaX proteins showed fluctuations between 1.5 and 5 Å across the trajectory (Fig. S4), consistent with the RMSD value observed during SN1382 interaction with the CoaX protein. Notably, while this interaction rigorously binds with the receptor pocket, and binding of the ligand compound does not alter the overall conformation of the CoaX protein (Fig. 4 and S4). Particularly, RMSF analysis revealed variations in the stability of different regions of the core CoaX protein. Specifically, residues 160–190 consistently displayed higher fluctuations across all four proteins (Fig. S4). Despite these fluctuations, it is worth highlighting that the crucial residues (active and binding site residues) of CoaX proteins maintained fluctuations of no more than 3 Å, emphasizing their considerable stability (Fig. S4). Furthermore, trajectory analysis provided insights into the underlying reasons for the fluctuations observed in the overall RMSD (1–5 Å) of CoaX proteins.

3.9.3. Trajectory analysis for tazobactam

The performance of tazobactam, a well-known broad-spectrum beta-lactamase inhibitor, was also evaluated across the 200 ns trajectory. The findings revealed that the RMSD value of each tazobactam-CoX complex fluctuated within the range of 1–5 Å, with certain segments of the complexes displaying some variations. Initially, the RMSD value for the tazobactam-CoaXb complex exhibited slightly broader fluctuations, reaching up to 7 Å, before decreasing to approximately 4 Å. Notably, the O2 atoms of tazobactam exhibited heightened polar affinities, particularly interacting strongly with ASN9 throughout the 200 ns simulation trajectory (Fig. S5A and File S2E). The binding affinities of the tazobactam to the functionally influential residues of CoaXb protein were formed through the H-bonding and water bridge formations. The compound tazobactam formed strong ionic and polar interaction with functionally important residues of CoaXd and CoaXp proteins, albeit displaying slightly higher RMSD fluctuations compared to the lead compound SN1382 (Fig. 4 and Figs. S5B-S5C). The strength between the interacting residues and tazobactam, along with the fluctuations of the complexes is presented in the accompanying animation file (File S2E-H). The only inconsistency observed was the

Fig. 4. Trajectory analysis for SN1382 (Vibegron)-CoaX complexes. A, B, C, and D respectively present the RMSD value of SN1382-CoXb, SN1382-CoXd, SN1382-CoXt, and SN1382-CoXp expressing the stability and dynamics of the complex over the 200 ns simulation. Subsequent figures put the interaction and binding affinities of ligands with protein residues on view. Lastly, RMSF describes the conformational changes of protein corresponding to the ligand.

interaction of tazobactam with the CoaXt protein, which exhibited unstable binding (File S2H).

3.10. Binding free energy of the drug candidates

The MM-GBSA method was employed to evaluate five important binding affinities from the trajectories of the SN1382-CoaX and tazobactam-CoaX complexes. Changes in Gibbs free energy on account of a protein and a ligand interaction of each complex were attained. The calculated alteration in Gibbs free energy during binding (r_psp_MMGBSA_dG_Bind) exhibited a negative value for every ligand-protein complex (Fig. 5). A negative ΔG implies that the formation of the complex releases more free energy than it consumes, indicating that the reaction occurs spontaneously. In the following analysis, the overall binding free energy, incorporating the influence of H-bonding with electronegative atoms (commonly nitrogen, oxygen, or fluorine), was similarly found to be negative (Fig. 5). Another prominent parameter was Bind Solv GB effects of solvent molecules on the energetics of the system were positive for all complexes. Finally, the two other critical parameters, coulombic and lipophilic effects on the binding free energy of the system, were calculated as negative (Fig. 5).

3.11. Agonist activity of SN1382 (Vibegron)

During molecular screening, Vibegron exhibited a release of approximately 10 kcal/mol against CoaX proteins in each instance. However, when screened against the beta-3 adrenergic receptor (PDB ID 7DH5), Vibegron only demonstrated an 8 kcal/mol release of free energy. The molecular dynamics analysis of the Vibegron and 7dh5 complex revealed that Vibegron initially prompted structural alterations within the adrenergic receptor, which remained relatively consistent throughout the extended trajectory time (Fig. S7A). Notably, the interaction between the receptor and Vibegron primarily involved strong hydrophobic interactions, with no significant covalent bonding observed during the 200 ns simulation (Fig. S7B). Nonetheless, the binding of the drug compound led to discernible conformational changes in the protein.

4. Discussion

In the last two decades, there has been a notable increase in the morbidity and mortality rates associated with clostridial infections across community and hospital settings (Goudarzi et al., 2014). This concerning trend is further compounded by the emergence of antibiotic-resistant strains and the resurgence of infections caused by four *Clostridium* species namely, *C. botulinum, C. difficile, C. tetani,* and *C. perfringens*, posing a significant challenge to public health. The limited availability of effective treatment options for moderate to severe cases exacerbates the urgency of addressing this issue. In this study, we report a novel discovery of a common drug target, type III CoaX, shared among four pathogenic *Clostridium* species (*C. botulinum, C. difficile, C. tetani,* and *C. perfringens*), utilizing core genomic approaches. Particularly intriguing is our observation of the inhibitory effects of SN1382 (Vibegron), a well-known agonist compound (CID: 137908674), on the newly identified CoaX target. Vibegron, initially developed and discovered by Merck, is a selective β3-adrenoreceptor agonist, first approved in Japan in September 2018 and subsequently in the United States in December 2020 for treating overactive bladder (Edmondson et al., 2016; Gleicher et al., 2022; Peyronnet et al., 2018). Our investigation revealed that Vibegron binds to the critical active and binding site of the CoaX protein, disrupting substrate and ion binding necessary for CoaX activity (Fig. 3 and File S2A-D). Notably, Vibegron's interaction mechanism differs, as it exclusively interacts with adrenergic receptors via hydrophobic interactions, inducing conformational changes within the receptor, akin to typical agonist compounds (McDonald & Lambert, 2022). Our study marks the first report of Vibegron's inhibitory activity, despite its existing availability in the market as an agonist drug. Additionally, we demonstrate the inhibitory effects of beta-lactamase (tazobactam) on CoaX, further expanding our understanding of potential therapeutic targets.

In this *in silico* study, we meticulously conducted step-by-step analyses to identify an optimal drug target suitable for designing *Closterium*-specific medications. Employing a core genomic approach, we scrutinized the entire genomes of *C. botulinum, C. difficile, C. tetani,* and *C. perfringens* to unveil shared drug targets. All necessary steps were taken to get a novel drug target for the top most pathogenic species of the genus *Clostridium* [70]. During our analysis, we ensured that the final novel drug target (CoaX), bears no resemblance to host proteins and has no association with human pathways. Similarly, several established studies have emphasized the bacterial type III CoaX as an appealing drug target because of its role in coenzyme A (CoA) biosynthesis and its dissimilarity to human pantothenate kinase [71,72]. While other kinase proteins exist in *Clostrisium*, type III pantothenate kinase emerges as the prime candidate meeting all criteria as a potential drug target in this current investigation [73]. Specific drugs targeting certain pathogenic *Clostridium* species are lacking; most drugs used against *Clostridium* are broad-spectrum. However, using broad-spectrum drugs for clostridial infections is unfavorable because they can target cell wall proteins, leading to bacterial cell wall lysis and release of toxins usually lethal for hosts [74,75]. The subcellular localization analysis confirmed that CoaX is located in the cytoplasm. Although membrane proteins are typically favored as drug targets, in the context of *Clostridium*, it may permissible to overlook them [75,76]. All physicochemical parameters pointed towards CoaX as a promising drug target for inhibiting the metabolic activities of chosen clostridial species [77]. The only oddness was that CoaXp was a little more hydrophilic in nature based on its GRAVY score. Hydrophobicity helps drug molecules access the target easily. Besides, orally available drugs usually have higher hydrophobicity [78,79]. Given the promising characteristics of the drug target, we proceeded with additional analysis on CoaX proteins. Another crucial aspect of CoaX was that all its proteins share common drug-binding pockets, with all active and binding site residues located within these pocket regions (Fig. 2). This increases the likelihood of a single drug being able to inhibit the CoaX activity across four distinct bacterial species [80].
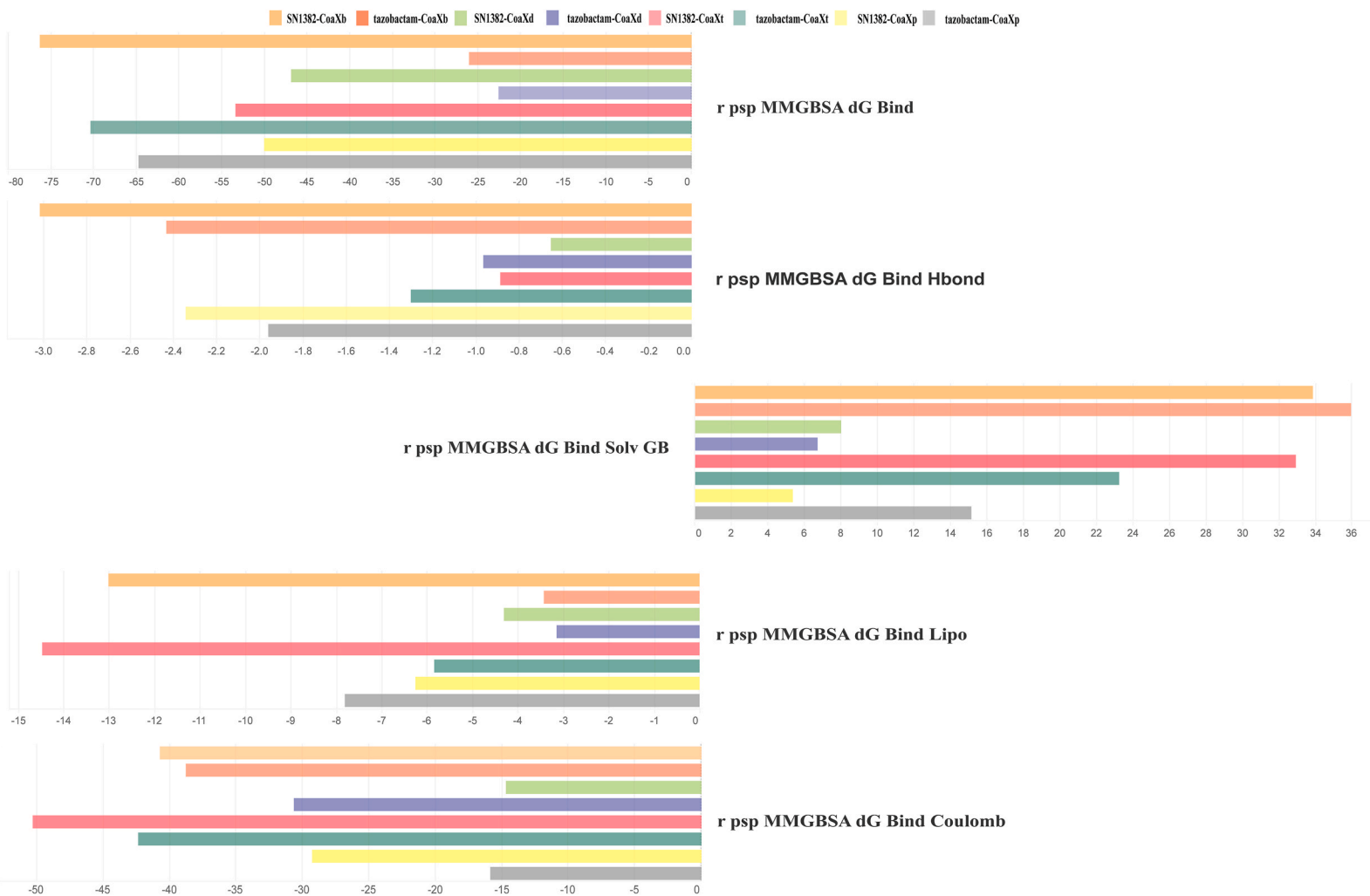
Fig. 5. Post simulation thermal MM-GBSA analysis for SN1382 and tazobactam. A total of five most prominent parameters presented the thermodynamical conditions of both inhibitory compounds when interacting with CoaX proteins.

Bacterial CoaX has appeared as a target of curiosity to break off the biosynthesis of coenzyme A and its distinctiveness from human pantothenate kinase [81–83]. CoaX is also an essential enzyme for *Clostridium*; it converts pantothenate into 4′-phospho-pantothenate (Fig. S6), which further converts into a CoA [84]. Pantothenate (vitamin B5) is fundamental for bacterial growth and cellular activity [85]. So, targeting the CoaX protein could be a promising choice to prevent the normal cellular function of clostridial pathogens. Pantothenate metabolism has been previously found to be a drug target for *Mycobacterium tuberculosis* [86]. Few studies have stated CoaX as a potential drug target against bacteria such as *Staphylococcus aureus* and *Acinetobacter baumannii* [71,87]. A computational approach is also taken to find new narrow or broad-spectrum antimicrobial agents against CoaX [88]. However, no previous study revealed CoaX as a potential drug target protein against *Clostridium*.

In this study, 1201 compounds were screened against the four identified CoaX proteins. Large-scale screening studies helped shortlist potential inhibitory compounds against the target. Detailed investigations into the changes in surface topology revealed that regions formed by H-bonding were crucial for robust receptor-ligand interaction. H-bonds are regarded as facilitators of protein-ligand binding alongside fundamental molecular descriptors to predict the oral bioavailability of small drug candidates [89,90]. An important interpretation was that the H-bonds topology of CoaXp was different, and a smaller number of H-bonds were demonstrated with each top free energy-releasing inhibitor compared to other CoaX proteins (Fig. 3). The oddness of the CoaXp protein was slightly hydrophilicity compared to others (Table 1). Furthermore, the logP values for the top nine compounds indicated hydrophobic nature (Table 3). However, hydrophobic inhibitors may not perform well against hydrophilic proteins [91], potentially causing differences in the hydrogen bond surface topology of CoaXp. Although the released free energies were similar, closer examination revealed disparities in intramolecular bindings (Table 1 and Fig. 3). Tazobactam (logP = 1.42) displayed a different surface topology of CoaXp compared to SN1382, with robust H-bonding with CoaXp.

In contemporary drug development, MDS have demonstrated significant utility [92]. In our analysis, we meticulously assessed each step of MDS since molecular screening alone may not offer comprehensive insight into protein-ligand complexes, as also suggested in previous studies [93]. The outcome of MDS revealed that H-bonds have a prominent effect on the stability of protein-ligand complexes. The RMSD fluctuations were less for the complexes with more H-bonds. The simulation Interaction Diagram (SID) framework enables us to comprehensively assess the properties of each receptor-ligand complex throughout the 200 ns trajectory. Through SID, we assessed five crucial criteria: stability, binding affinity, conformational changes, interactions, and dynamics of every receptor-ligand complex. This comprehensive method contributed to a deep understanding of the complex dynamics and interactions within the protein-ligand systems. SN1382 exhibited satisfactory interactions with functionally active and binding residues of CoaXb, CoaXd, and CoXt. Despite overall RMSD fluctuations ranging from 1 to 5 Å for each protein-ligand complex (Fig. 4), residues interacting with lead compounds showed fluctuations up to 3 Å, which is deemed perfectly acceptable [94]. This is because interacting ligand atoms with protein residues maintained uninterrupted interactions throughout dynamic periods (File S2A-C). In particular, residues exhibiting strong interactions with ligands demonstrated fluctuations of 1–3 Å in RMSF diagrams, supporting the likelihood of higher average RMSD values. Each of the RMSF diagrams exhibited residues from 160 to 190 regions with higher fluctuations (Fig. 4). Once again, a 200 ns simulation for each blank CoaX protein (only protein with no ligand) was performed to draw a more precise conclusion about the higher overall RMSD value. It was clear that the reason for the overall slightly higher RMSD value was the 160–190 region of the CoaX proteins. The most acceptable reason is that the structure of CoaX proteins was developed based on the homology of CoaX from *Bacillus anthracis*. Residues that fall between 160 and 190 regions possess significant differences with reference structure, and higher fluctuations in RMSF were also observed in these regions (Fig. 4 and Fig. S4). Although residues within the 160–190 regions do not significantly affect ligand binding, they contribute to the overall RMSD. Initial analysis of the protein structures indicated acceptable quality, yet MDS offered detailed insights into their structure (Figs. S2 and S4). In our analysis, we revealed that the inhibitory compound SN1382 exhibited strong affinities to crucial residues of CoaX proteins, except CoaXp, indicating that the ligand created a suitable environment during interaction with the protein (Fig. 4 and Fig. S4).

We incorporated a known commercially available drug, tazobactam, which reported inhibitory activity against *Clostridium* [13,95]. Tazobactam, commonly known as a beta-lactamase inhibitor, and its specificity against CoaX protein have not been revealed in any literature. As our prepared library compounds have slightly higher logP values, thus we consider tazobactam, which has a lower logP value compared to the top free energy-providing inhibitory compounds of this study (Table 3). Surprisingly, the highest number of H-bonds were observed in between the tazobactam-CoaXp complex (Fig. S3). In MDS, tazobactam displayed interaction with functionally important residues with overall RMSD fluctuations 1–7 Å (Fig. S5). Similar RMSF fluctuations were seen in the 160–190 residual position in all tazobactam-CoaX complexes, while strong binding affinities were observed with all CoaX proteins except CoaXt, where unstable binding affinities were noted over the 200 ns trajectory (File S2G). Earlier studies reported the inhibitory activity of tazobactam against *C. botulinum*, *C. difficile*, and *C. perfringens*, aligning with our findings of robust binding affinities with tazobactam. While tazobactam has shown a clostridiocidal effect against *C. botulinum*, we found adequate performance of SN1382 against CoaXb. Interestingly, simulation results of the SN1382-CoaXp complex revealed less favorable interactions with crucial residues of CoaXp, contrasting with tazobactam's robust interactions with important amino acid residues (File S2H), suggesting that tazobactam may overcome the weak performance of SN1382 against CoaXp. To know the binding thermodynamics of SN1382 and tazobactam the comparison of thermal MM-GBSA analysis was made on the performance of SN1382 and tazobactam against each CoaX protein. The comparisons of total binding free energy (dG Bind) [96] indicate that SN1382 could be a better inhibitor for CoaXb, CoaXd and CoaXt. For CoaXp, tazobactam would be a better option. The other three parameters, dG Bind Hbond, Bind lipo, and bind coulomb, pinpointed that the SN1382 and tazobactam released free energies interacting with CoaX proteins. In some cases, SN1382 performed better against target proteins than tazobactam and vice versa (Fig. 5). A remarkable point was that the solvent effect (dG Bind Solv GB) on our proposed inhibitory compound SN1382 was positive against CoaX protein. The positive score indicated that the inhibitory compound SN1382 could not readily dissolve in water when interacting with the target protein [97]. The comparative thermal MM-GBSA analysis

pointed out that both the SN1382 and tazobactam are suitable against the target, though in some cases, one releases higher free energies than the other. The only exception was that the inhibitory activity of SN1382 against CoaXp was also poor in thermal MM-GBSA analysis. However, tazobactam had more significant affinities for CoaXp rather than SN1382. Besides, the simulation trajectory showed that tazobactam performed well against CoaXb and CoaXd. Consequently, we identify a beta-lactamase inhibitor, tazobactam, as a potential CoaX inhibitor based on this computational study. The overall performance of both SN1382 and tazobactam was satisfactory, while SN1382 performed poorly against CoaXp and tazobactam against CoaXt. The fewer fluctuations with the critical residues glimpsed SN1382 might be a suitable inhibitor against three CoaX proteins. Besides, its hydrophobic nature would be fair in not breaking the cell membrane, which ultimately helps to overcome the clostridiocidal effects of currently available drugs [98]. However, tazobactam is known as a beta-lactamase inhibitor. Still, it is commonly used in *Clostridium* treatment, and our *in silico* study revealed its affinities to CoaX are a matter of curiosity. Our findings propose that a combination of these two compounds (Vibegron + tazobactam) could effectively inhibit the activity of four pathogenic *Clostridium* species. Further experimental studies present a promising avenue for future research and therapeutic development.

5. Conclusion

In summary, this study identified type III pantothenate kinase (CoaX) as a shared drug target across four pathogenic Clostridium species viz. *botulinum, C. difficile, C. tetani*, and *C. perfringens*—using a core genomic approach. This discovery represents a significant advancement in the search for new antimicrobial agents against clostridial infections. CoaX, with its specificity and ability to avoid the lytic effects of antibiotics, offers a promising path for developing therapies against antibiotic-resistant Clostridium infections. The inhibitory effects of Vibegron on CoaX proteins further support this approach. Targeting a single drug that combats all four clostridial pathogens is economically advantageous, streamlining pharmaceutical development and production. This universal therapeutic option improves access to effective treatments for a wide range of clostridial infections, benefiting patients and healthcare systems. Future research should focus on optimizing CoaX inhibitors, understanding resistance mechanisms, conducting preclinical and clinical trials, exploring combination therapies, and monitoring epidemiological trends. These efforts are crucial for advancing treatment options and addressing emerging challenges in managing clostridial infections, ultimately improving patient outcomes and public health.

Consent for publication

Not applicable.

CRediT authorship contribution statement

Soharth Hasnat: Writing – original draft, Visualization, Software, Methodology, Formal analysis, Data curation, Conceptualization. **M. Nazmul Hoque:** Writing – review & editing, Supervision, Software, Resources, Project administration, Methodology, Formal analysis, Conceptualization. **M Murshida Mahbub:** Writing – original draft, Validation, Supervision, Resources, Investigation, Conceptualization. **Tahsin Islam Sakif:** Writing – review & editing, Validation, Software, Methodology, Formal analysis, Data curation. **A.D.A. Shahinuzzaman:** Visualization, Validation, Software, Methodology, Investigation, Formal analysis. **Tofazzal Islam:** Writing – review & editing, Supervision, Resources, Conceptualization.

Declaration of competing interest

The authors declare that they have no known competing financial interests or personal relationships that could have appeared to influence the work reported in this paper.

Appendix A. Supplementary data

Supplementary data to this article can be found online at https://doi.org/10.1016/j.heliyon.2024.e34544.

References

[1] A.C. Parte, LPSN–list of prokaryotic names with standing in nomenclature, Epub 20131115, Nucleic Acids Res. 42 (Database issue) (2014) D613–D616, https://doi.org/10.1093/nar/gkt1111. PubMed PMID: 24243842; PubMed Central PMCID: PMCPMC3965054.

[2] G.P. Carter, J.K. Cheung, S. Larcombe, D. Lyras, Regulation of toxin production in the pathogenic clostridia, Mol. Microbiol. 91 (2) (2014) 221–231, https://doi.org/10.1111/mmi.12469. PubMed PMID: 24563915.

[3] B. Hassel, Tetanus: pathophysiology, treatment, and the possibility of using botulinum toxin against tetanus-induced rigidity and spasms, Epub 20130108, Toxins 5 (1) (2013) 73–83, https://doi.org/10.3390/toxins5010073. PubMed PMID: 23299659; PubMed Central PMCID: PMCPMC3564069.

[4] M.M. Saleh, A.L. Frisbee, J.L. Leslie, E.L. Buonomo, C.A. Cowardin, J.Z. Ma, et al., Colitis-Induced Th17 cells increase the risk for subsequent Clostridium difficile infection, 65.e5, Cell Host Microbe 25 (5) (2019) 756, https://doi.org/10.1016/j.chom.2019.03.003. PubMed PMID: 31003940.

[5] E. Finn, F.L. Andersson, M. Madin-Warburton, Burden of Clostridioides difficile infection (CDI) - a systematic review of the epidemiology of primary and recurrent CDI, BMC Infect. Dis. 21 (1) (2021) 456, https://doi.org/10.1186/s12879-021-06147-y.

[6] J. Li, Z. Liu, C. Yu, K. Tan, S. Gui, S. Zhang, Y. Shen, Global epidemiology and burden of tetanus from 1990 to 2019: a systematic analysis for the Global Burden of Disease Study 2019, Epub 20230421, Int. J. Infect. Dis. 132 (2023) 118–126, https://doi.org/10.1016/j.ijid.2023.04.402. PubMed PMID: 37086867.

[7] P. Feuerstadt, N. Theriault, G. Tillotson, The burden of CDI in the United States: a multifactorial challenge, BMC Infect. Dis. 23 (1) (2023) 132, https://doi.org/10.1186/s12879-023-08096-0.

[8] J.E. Cohen, R. Wang, R.F. Shen, W.W. Wu, J.E. Keller, Comparative pathogenomics of Clostridium tetani, Epub 20170811, PLoS One 12 (8) (2017) e0182909, https://doi.org/10.1371/journal.pone.0182909. PubMed PMID: 28800585; PubMed Central PMCID: PMCPMC5553647.

[9] H. Hanif, A. Anjum, N. Ali, A. Jamal, M. Imran, B. Ahmad, M.I. Ali, Isolation and antibiogram of Clostridium tetani from clinically diagnosed tetanus patients, The American Society of Tropical Medicine and Hygiene 93 (4) (2015) 752–756, https://doi.org/10.4269/ajtmh.15-0040.

[10] H.J. Song, K.N. Shim, S.A. Jung, H.J. Choi, M.A. Lee, K.H. Ryu, et al., Antibiotic-associated diarrhea: candidate organisms other than Clostridium difficile, Korean J. Intern. Med. (Engl. Ed.) 23 (1) (2008) 9–15, https://doi.org/10.3904/kjim.2008.23.1.9. PubMed PMID: 18363274; PubMed Central PMCID: PMCPMC2686956.

[11] C. Lúquez, L. Edwards, C. Griffin, J. Sobel, Foodborne botulism outbreaks in the United States, 2001-2017, Epub 20210716, Front. Microbiol. 12 (2021) 713101, https://doi.org/10.3389/fmicb.2021.713101. PubMed PMID: 34335550; PubMed Central PMCID: PMCPMC8322756.

[12] J.B.M.-L.H. Buboltz, Gas gangrene, in: Gas Gangrene [Internet]. Treasure Island, StatPearls [Internet], 2023. Available from: https://www.ncbi.nlm.nih.gov/books/NBK537030/.

[13] M. Li, N. Li, Clostridium perfringens bloodstream infection secondary to acute pancreatitis: a case report, World J Clin Cases 9 (17) (2021) 4357–4364, https://doi.org/10.12998/wjcc.v9.i17.4357. PubMed PMID: 34141801; PubMed Central PMCID: PMCPMC8173429.

[14] M. Mohi Ud Din, Z. Iqbal, M. Farooq, M. Mansoor, R. Sawar, A. Mohiud Din, et al., MULTIDRUG RESISTANCE IN CLOSTRIDIA, 2022.

[15] Proceedings of the 2006 ACM/IEEE Conference on Supercomputing, Association for Computing Machinery, Tampa, Florida, 2006.

[16] S. Jackowski, C. Rock, Regulation of coenzyme A biosynthesis, J. Bacteriol. 148 (3) (1981) 926–932.

[17] J.C. Evans, C. Trujillo, Z. Wang, H. Eoh, S. Ehrt, D. Schnappinger, et al., Validation of CoaBC as a bactericidal target in the coenzyme A pathway of Mycobacterium tuberculosis, ACS Infect. Dis. 2 (12) (2016) 958–968.

[18] L.R. Chiarelli, G. Mori, B.S. Orena, M. Esposito, T. Lane, A.L. de Jesus Lopes Ribeiro, et al., A multitarget approach to drug discovery inhibiting Mycobacterium tuberculosis PyrG and PanK, Sci. Rep. 8 (1) (2018) 3187, https://doi.org/10.1038/s41598-018-21614-4.

[19] D. Awasthy, A. Ambady, J. Bhat, G. Sheikh, S. Ravishankar, V. Subbulakshmi, et al., Essentiality and functional analysis of type I and type III pantothenate kinases of Mycobacterium tuberculosis, Epub 20100624, Microbiology (Read.) 156 (Pt 9) (2010) 2691–2701, https://doi.org/10.1099/mic.0.040717-0. PubMed PMID: 20576686.

[20] A. Dereeper, M. Summo, D.F. Meyer, PanExplorer: a web-based tool for exploratory analysis and visualization of bacterial pan-genomes, Bioinformatics 38 (18) (2022) 4412–4414, https://doi.org/10.1093/bioinformatics/btac504.

[21] Y. Zhao, J. Wu, J. Yang, S. Sun, J. Xiao, J. Yu, PGAP: pan-genomes analysis pipeline, Bioinformatics 28 (3) (2011) 416–418, https://doi.org/10.1093/bioinformatics/btr655.

[22] M. Johnson, I. Zaretskaya, Y. Raytselis, Y. Merezhuk, S. McGinnis, T.L. Madden, NCBI blast: a better web interface, Nucleic Acids Res. 36 (suppl_2) (2008) W5–W9, https://doi.org/10.1093/nar/gkn201.

[23] F.S. Collins, L. Fink, The human genome Project, Alcohol Health Res. World 19 (3) (1995) 190–195. PubMed PMID: 31798046; PubMed Central PMCID: PMCPMC6875757.

[24] S.A. Muhammad, S. Ahmed, A. Ali, H. Huang, X. Wu, X.F. Yang, et al., Prioritizing drug targets in Clostridium botulinum with a computational systems biology approach, Genomics 104 (1) (2014) 24–35, https://doi.org/10.1016/j.ygeno.2014.05.002.

[25] S.I. Mondal, S. Ferdous, N.A. Jewel, A. Akter, Z. Mahmud, M.M. Islam, et al., Identification of potential drug targets by subtractive genome analysis of Escherichia coli O157:H7: an in silico approach, Epub 20151208, Adv Appl Bioinform Chem 8 (2015) 49–63, https://doi.org/10.2147/aabc.S88522. PubMed PMID: 26677339; PubMed Central PMCID: PMCPMC4677596.

[26] H. Saleem, U.A. Ashfaq, H. Nadeem, M. Zubair, M.H. Siddique, I. Rasul, Subtractive genomics and molecular docking approach to identify drug targets against Stenotrophomonas maltophilia, Epub 20211215, PLoS One 16 (12) (2021) e0261111, https://doi.org/10.1371/journal.pone.0261111. PubMed PMID: 34910751; PubMed Central PMCID: PMCPMC8673605.

[27] J. Pevsner, Bioinformatics and Functional Genomics, John Wiley & Sons, 2015.

[28] V. Veeramachaneni, W. Makałowski, Visualizing sequence similarity of protein families, Epub 20040512, Genome Res. 14 (6) (2004) 1160–1169, https://doi.org/10.1101/gr.2079204. PubMed PMID: 15140831; PubMed Central PMCID: PMCPMC419794.

[29] M. Kilinc, K. Jia, R.L. Jernigan, Improved global protein homolog detection with major gains in function identification, Epub 20230224, Proc. Natl. Acad. Sci. U.S.A. 120 (9) (2023) e2211823120, https://doi.org/10.1073/pnas.2211823120. PubMed PMID: 36827259; PubMed Central PMCID: PMCPMC9992864.

[30] J. Deng, L. Deng, S. Su, M. Zhang, X. Lin, L. Wei, et al., Investigating the predictability of essential genes across distantly related organisms using an integrative approach, Nucleic Acids Res. 39 (3) (2010) 795–807, https://doi.org/10.1093/nar/gkq784.

[31] R. Zhang, H.Y. Ou, C.T. Zhang, DEG: a database of essential genes, Nucleic Acids Res. 32 (suppl_1) (2004) D271–D272, https://doi.org/10.1093/nar/gkh024.

[32] Y. Moriya, M. Itoh, S. Okuda, A.C. Yoshizawa, M. Kanehisa, KAAS: an automatic genome annotation and pathway reconstruction server, Nucleic Acids Res. 35 (suppl_2) (2007) W182–W185, https://doi.org/10.1093/nar/gkm321.

[33] D.S. Wishart, Y.D. Feunang, A.C. Guo, E.J. Lo, A. Marcu, J.R. Grant, et al., DrugBank 5.0: a major update to the DrugBank database for 2018, d82, Nucleic Acids Res. 46 (D1) (2018) D1074, https://doi.org/10.1093/nar/gkx1037. PubMed PMID: 29126136; PubMed Central PMCID: PMCPMC5753335.

[34] B.P. Alcock, A.R. Raphenya, T.T.Y. Lau, K.K. Tsang, M. Bouchard, A. Edalatmand, et al., Card 2020: antibiotic resistome surveillance with the comprehensive antibiotic resistance database, Nucleic Acids Res. 48 (D1) (2019) D517–D525, https://doi.org/10.1093/nar/gkz935.

[35] L. Chen, J. Yang, J. Yu, Z. Yao, L. Sun, Y. Shen, Q. Jin, VFDB: a reference database for bacterial virulence factors, Nucleic Acids Res. 33 (suppl_1) (2005) D325–D328, https://doi.org/10.1093/nar/gki008.

[36] K.R. Sakharkar, M.K. Sakharkar, V.T. Chow, Biocomputational strategies for microbial drug target identification, Methods Mol. Med. 142 (2008) 1–9, https://doi.org/10.1007/978-1-59745-246-5_1. PubMed PMID: 18437301.

[37] A.R. Oany, M. Mia, T. Pervin, M.N. Hasan, A. Hirashima, Identification of potential drug targets and inhibitor of the pathogenic bacteria Shigella flexneri 2a through the subtractive genomic approach, In Silico Pharmacology 6 (1) (2018) 11, https://doi.org/10.1007/s40203-018-0048-2.

[38] N.Y. Yu, J.R. Wagner, M.R. Laird, G. Melli, S. Rey, R. Lo, et al., PSORTb 3.0: improved protein subcellular localization prediction with refined localization subcategories and predictive capabilities for all prokaryotes, Bioinformatics 26 (13) (2010) 1608–1615, https://doi.org/10.1093/bioinformatics/btq249.

[39] H.B. Shen, K.C. Chou, Gpos-mPLoc: a top-down approach to improve the quality of predicting subcellular localization of Gram-positive bacterial proteins, Protein Pept. Lett. 16 (12) (2009) 1478–1484, https://doi.org/10.2174/092986609789839322. PubMed PMID: 20001911.

[40] H. Kaur, M. Kalia, N. Taneja, Identification of novel non-homologous drug targets against Acinetobacter baumannii using subtractive genomics and comparative metabolic pathway analysis, Epub 20201107, Microb. Pathog. 152 (2021) 104608, https://doi.org/10.1016/j.micpath.2020.104608. PubMed PMID: 33166618.

[41] F. Shahid, U.A. Ashfaq, S. Saeed, S. Munir, A. Almatroudi, M. Khurshid, In silico subtractive proteomics approach for identification of potential drug targets in Staphylococcus saprophyticus, Epub 20200522, Int. J. Environ. Res. Publ. Health 17 (10) (2020), https://doi.org/10.3390/ijerph17103644. PubMed PMID: 32455889; PubMed Central PMCID: PMCPMC7277342.

[42] E. Gasteiger, C. Hoogland, A. Gattiker, Se Duvaud, M.R. Wilkins, R.D. Appel, A. Bairoch, Protein identification and analysis tools on the ExPASy server, in: J. M. Walker (Ed.), The Proteomics Protocols Handbook, Humana Press, Totowa, NJ, 2005, pp. 571–607.

[43] H.A. Dar, T. Zaheer, N. Ullah, S.M. Bakhtiar, T. Zhang, M. Yasir, et al., Pangenome analysis of Mycobacterium tuberculosis reveals core-drug targets and screening of promising lead compounds for drug discovery, Epub 20201117, Antibiotics 9 (11) (2020), https://doi.org/10.3390/antibiotics9110819. PubMed PMID: 33213029; PubMed Central PMCID: PMCPMC7698547.

[44] A. Fiser, A. Sali, Modeller: generation and refinement of homology-based protein structure models, Methods Enzymol. 374 (2003) 461–491, https://doi.org/10.1016/s0076-6879(03)74020-8. PubMed PMID: 14696385.

[45] S. Nair, N. Wadhwa, B. Singh, N. Arora, Identification of B Cell epitopes of alcohol dehydrogenase allergen of curvularia lunata, PLoS One 6 (2011) e20020, https://doi.org/10.1371/journal.pone.0020020.

[46] A. Messaoudi, H. Belguith, J. Ben Hamida, Homology modeling and virtual screening approaches to identify potent inhibitors of VEB-1 β-lactamase, Epub 20130402, Theor. Biol. Med. Model. 10 (2013) 22, https://doi.org/10.1186/1742-4682-10-22. PubMed PMID: 23547944; PubMed Central PMCID: PMCPMC3668210.

[47] A. Wlodawer, Stereochemistry and validation of macromolecular structures, Methods Mol. Biol. 1607 (2017) 595–610, https://doi.org/10.1007/978-1-4939-7000-1_24. PubMed PMID: 28573590; PubMed Central PMCID: PMCPMC5560084.

[48] E. Krieger, K. Joo, J. Lee, J. Lee, S. Raman, J. Thompson, et al., Improving physical realism, stereochemistry, and side-chain accuracy in homology modeling: four approaches that performed well in CASP8, Suppl 9, Proteins 77 (Suppl 9) (2009) 114–122, https://doi.org/10.1002/prot.22570. PubMed PMID: 19768677; PubMed Central PMCID: PMCPMC2922016.

[49] E. Krieger, G. Koraimann, G. Vriend, Increasing the precision of comparative models with YASARA NOVA–a self-parameterizing force field, Proteins 47 (3) (2002) 393–402, https://doi.org/10.1002/prot.10104. PubMed PMID: 11948792.

[50] K. Roy, S. Kar, R.N. Das, Chapter 5 - computational chemistry, in: K. Roy, S. Kar, R.N. Das (Eds.), Understanding the Basics of QSAR for Applications in Pharmaceutical Sciences and Risk Assessment, Academic Press, Boston, 2015, pp. 151–189.

[51] A. Volkamer, D. Kuhn, F. Rippmann, M. Rarey, DoGSiteScorer: a web server for automatic binding site prediction, analysis and druggability assessment, Bioinformatics 28 (15) (2012) 2074–2075, https://doi.org/10.1093/bioinformatics/bts310.

[52] N.I. Nicely, D. Parsonage, C. Paige, G.L. Newton, R.C. Fahey, R. Leonardi, et al., Structure of the type III pantothenate kinase from Bacillus anthracis at 2.0 Å resolution: implications for coenzyme A-dependent redox biology, Biochemistry 46 (11) (2007) 3234–3245, https://doi.org/10.1021/bi062299p.

[53] E.F. Pettersen, T.D. Goddard, C.C. Huang, G.S. Couch, D.M. Greenblatt, E.C. Meng, T.E. Ferrin, UCSF Chimera—a visualization system for exploratory research and analysis, J. Comput. Chem. 25 (13) (2004) 1605–1612, https://doi.org/10.1002/jcc.20084.

[54] P. Csizmadia (Ed.), MarvinSketch and MarvinView: Molecule Applets for the World Wide Web, 1999.

[55] M.D. Hanwell, D.E. Curtis, D.C. Lonie, T. Vandermeersch, E. Zurek, G.R. Hutchison, Avogadro: an advanced semantic chemical editor, visualization, and analysis platform, J. Cheminf. 4 (1) (2012) 17, https://doi.org/10.1186/1758-2946-4-17.

[56] L. Jaillet, S. Artemova, S. Redon, IM-UFF: extending the universal force field for interactive molecular modeling, J. Mol. Graph. Model. 77 (2017) 350–362, https://doi.org/10.1016/j.jmgm.2017.08.023.

[57] N. Engler, A. Ostermann, N. Niimura, F.G. Parak, Hydrogen atoms in proteins: positions and dynamics, Epub 20030822, Proc. Natl. Acad. Sci. U. S. A. 100 (18) (2003) 10243–10248, https://doi.org/10.1073/pnas.1834279100. PubMed PMID: 12937341; PubMed Central PMCID: PMCPMC193546.

[58] S.E. Wong, F.C. Lightstone, Accounting for water molecules in drug design, Epub 20101123, Expet Opin. Drug Discov. 6 (1) (2011) 65–74, https://doi.org/10.1517/17460441.2011.534452. PubMed PMID: 22646827.

[59] S. Forli, R. Huey, M.E. Pique, M.F. Sanner, D.S. Goodsell, A.J. Olson, Computational protein–ligand docking and virtual drug screening with the AutoDock suite, Nat. Protoc. 11 (5) (2016) 905–919, https://doi.org/10.1038/nprot.2016.051.

[60] N.M. O'Boyle, M. Banck, C.A. James, C. Morley, T. Vandermeersch, G.R. Hutchison, Open Babel: an open chemical toolbox, J. Cheminf. 3 (1) (2011) 33, https://doi.org/10.1186/1758-2946-3-33.

[61] S. Bouamrane, A. Khaldan, H. Hajji, R. El-Mernissi, M. Alaqarbeh, N. Alsakhen, et al., In silico identification of 1,2,4-triazoles as potential Candida Albicans inhibitors using 3D-QSAR, molecular docking, molecular dynamics simulations, and ADMET profiling, Epub 20221014, Mol. Divers. 27 (5) (2023) 2111–2132, https://doi.org/10.1007/s11030-022-10546-x. PubMed PMID: 36239842.

[62] C.A. Lobato-Tapia, Y. Moreno-Hernández, Z.E. Olivo-Vidal, In silico studies of four compounds of cecropia obtusifolia against malaria parasite, Epub 20231003, Molecules 28 (19) (2023), https://doi.org/10.3390/molecules28196912. PubMed PMID: 37836757; PubMed Central PMCID: PMCPMC10574735.

[63] X. Che, Q. Liu, L. Zhang, An accurate and universal protein-small molecule batch docking solution using Autodock Vina, Results in Engineering 19 (2023) 101335, https://doi.org/10.1016/j.rineng.2023.101335.

[64] L. Ivanova, M. Karelson, The impact of software used and the type of target protein on molecular docking accuracy, Epub 20221218, Molecules 27 (24) (2022), https://doi.org/10.3390/molecules27249041. PubMed PMID: 36558174; PubMed Central PMCID: PMCPMC9788237.

[65] BIOVIA, Dassault Systèmes, Discovery Studio 2024. v24.10, 23298 ed, Dassault Systèmes, San Diego, 2024.

[66] M.S. Badar, S. Shamsi, J. Ahmed, M.A. Alam, Molecular dynamics simulations: concept, methods, and applications, in: N. Rezaei (Ed.), Transdisciplinarity, Springer International Publishing, Cham, 2022, pp. 131–151.

[67] J.L. Banks, H.S. Beard, Y. Cao, A.E. Cho, W. Damm, R. Farid, et al., Integrated modeling program, applied chemical theory (IMPACT), J. Comput. Chem. 26 (16) (2005) 1752–1780, https://doi.org/10.1002/jcc.20292. PubMed PMID: 16211539; PubMed Central PMCID: PMCPMC2742605.

[68] C. Huang, C. Li, P.Y. Choi, K. Nandakumar, L.W. Kostiuk, A novel method for molecular dynamics simulation in the isothermal–isobaric ensemble, Mol. Phys. 109 (2) (2011) 191–202.

[69] Z. Jin, Y. Wang, X.-F. Yu, Q.-Q. Tan, S.-S. Liang, T. Li, et al., Structure-based virtual screening of influenza virus RNA polymerase inhibitors from natural compounds: molecular dynamics simulation and MM-GBSA calculation, Comput. Biol. Chem. 85 (2020) 107241, https://doi.org/10.1016/j.compbiolchem.2020.107241.

[70] N.A. Qureshi, S.M. Bakhtiar, M. Faheem, M. Shah, A. Bari, H.M. Mahmood, et al., Genome-based drug target identification in human pathogen Streptococcus gallolyticus, Epub 20210325, Front. Genet. 12 (2021) 564056, https://doi.org/10.3389/fgene.2021.564056. PubMed PMID: 33841489; PubMed Central PMCID: PMCPMC8027347.

[71] A. Singla, P. Sharma, A. Gupta, N. Iqbal, C. Rani, T.P. Singh, S. Sharma, Biophysical characterization of type III pantothenate kinase (PanK) from acinetobacter baumannii, Protein Pept. Lett. 28 (4) (2021) 450–458, https://doi.org/10.2174/0929866527666200813202445. PubMed PMID: 32798368.

[72] K. Yang, Y. Eyobo, L.A. Brand, D. Martynowski, D. Tomchick, E. Strauss, H. Zhang, Crystal structure of a type III pantothenate kinase: insight into the mechanism of an essential coenzyme A biosynthetic enzyme universally distributed in bacteria, J. Bacteriol. 188 (15) (2006) 5532–5540, https://doi.org/10.1128/jb.00469-06. PubMed PMID: 16855243; PubMed Central PMCID: PMCPMC1540032.

[73] O. Masataka, N. Masahiro, K. Keiko, S. Jun, Role of tyrosine kinase A receptor (TrkA) on pathogenicity of Clostridium perfringens alpha-toxin, in: H. Cai (Ed.), Protein Phosphorylation in Human Health, Rijeka: IntechOpen, 2012. Ch. 11.

[74] P. Sarkar, V. Yarlagadda, C. Ghosh, J. Haldar, A review on cell wall synthesis inhibitors with an emphasis on glycopeptide antibiotics, Epub 20170126, Medchemcomm 8 (3) (2017) 516–533, https://doi.org/10.1039/c6md00585c. PubMed PMID: 30108769; PubMed Central PMCID: PMCPMC6072328.

[75] J.R. Barash, J.B. Castles, S.S. Arnon, Antimicrobial susceptibility of 260 Clostridium botulinum type A, B, Ba, and bf strains and a neurotoxigenic Clostridium baratii type F strain isolated from California infant botulism patients, Antimicrob. Agents Chemother. 62 (12) (2018), https://doi.org/10.1128/aac.01594-18, 10.1128/aac.01594-18.

[76] M.I. Hosen, A.M. Tanmoy, D.-A. Mahbuba, U. Salma, M. Nazim, M.T. Islam, S. Akhteruzzaman, Application of a subtractive genomics approach for in silico identification and characterization of novel drug targets in Mycobacterium tuberculosis F11, Interdiscip. Sci. Comput. Life Sci. 6 (1) (2014) 48–56, https://doi.org/10.1007/s12539-014-0188-y.

[77] K.Y. Chang, J.R. Yang, Analysis and prediction of highly effective antiviral peptides based on random forests, Epub 20130805, PLoS One 8 (8) (2013) e70166, https://doi.org/10.1371/journal.pone.0070166. PubMed PMID: 23940542; PubMed Central PMCID: PMCPMC3734225.

[78] S.C. Bull, A.J. Doig, Properties of protein drug target classes, Epub 20150330, PLoS One 10 (3) (2015) e0117955, https://doi.org/10.1371/journal.pone.0117955. PubMed PMID: 25822509; PubMed Central PMCID: PMCPMC4379170.

[79] J. Zuegg, M.A. Cooper, Drug-likeness and increased hydrophobicity of commercially available compound libraries for drug screening, Curr. Top. Med. Chem. 12 (14) (2012) 1500–1513, https://doi.org/10.2174/156802612802652466. PubMed PMID: 22827520.

[80] S. Panda, G. Chandra, Physicochemical characterization and functional analysis of some snake venom toxin proteins and related non-toxin proteins of other chordates, Epub 20120921, Bioinformation 8 (18) (2012) 891–896, https://doi.org/10.6026/97320630008891. PubMed PMID: 23144546; PubMed Central PMCID: PMCPMC3489095.

[81] A. Nurkanto, G. Jeelani, H.J. Santos, Y. Rahmawati, M. Mori, Y. Nakamura, et al., Characterization of plasmodium falciparum pantothenate kinase and identification of its inhibitors from natural products, Epub 20210309, Front. Cell. Infect. Microbiol. 11 (2021) 639065, https://doi.org/10.3389/fcimb.2021.639065. PubMed PMID: 33768012; PubMed Central PMCID: PMCPMC7985445.

[82] H.S. Butman, T.J. Kotzé, C.S. Dowd, E. Strauss, Vitamin in the crosshairs: targeting pantothenate and coenzyme A biosynthesis for new antituberculosis agents, Epub 20201215, Front. Cell. Infect. Microbiol. 10 (2020) 605662, https://doi.org/10.3389/fcimb.2020.605662. PubMed PMID: 33384970; PubMed Central PMCID: PMCPMC7770189.

[83] C. Spry, K. Kirk, K.J. Saliba, Coenzyme A biosynthesis: an antimicrobial drug target, FEMS Microbiol. Rev. 32 (1) (2008) 56–106, https://doi.org/10.1111/j.1574-6976.2007.00093.x. PubMed PMID: 18173393.

[84] A. Czumaj, S. Szrok-Jurga, A. Hebanowska, J. Turyn, J. Swierczynski, T. Sledzinski, E. Stelmanska, The pathophysiological role of CoA, Epub 20201128, Int. J. Mol. Sci. 21 (23) (2020), https://doi.org/10.3390/ijms21239057. PubMed PMID: 33260564; PubMed Central PMCID: PMCPMC7731229.

[85] A.C. Murillo, H.Y. Li, T. Alber, E.N. Baker, J.M. Berger, L.T. Cherney, et al., High throughput crystallography of TB drug targets, Infect. Disord.: Drug Targets 7 (2) (2007) 127–139, https://doi.org/10.2174/187152607781001853. PubMed PMID: 17970224.

[86] E.L. White, K. Southworth, L. Ross, S. Cooley, R.B. Gill, M.I. Sosa, et al., A novel inhibitor of Mycobacterium tuberculosis pantothenate synthetase, Epub 20061214, J. Biomol. Screen 12 (1) (2007) 100–105, https://doi.org/10.1177/1087057106296484. PubMed PMID: 17175524.

[87] A.E. Choudhry, T.L. Mandichak, J.P. Broskey, R.W. Egolf, C. Kinsland, T.P. Begley, et al., Inhibitors of pantothenate kinase: novel antibiotics for staphylococcal infections, Antimicrob. Agents Chemother. 47 (6) (2003) 2051–2055, https://doi.org/10.1128/aac.47.6.2051-2055.2003.

[88] S.E. Brigg, L. Koekemoer, L.A. Brand, E. Strauss, Multifaceted target specificity analysis as a tool in antimicrobial drug development: type III pantothenate kinases as a case study, Epub 20230222, ChemMedChem 18 (7) (2023) e202200630, https://doi.org/10.1002/cmdc.202200630. PubMed PMID: 36749500.

[89] J.T.S. Coimbra, R. Feghali, R.P. Ribeiro, M.J. Ramos, P.A. Fernandes, The importance of intramolecular hydrogen bonds on the translocation of the small drug piracetam through a lipid bilayer, Epub 20210104, RSC Adv. 11 (2) (2020) 899–908, https://doi.org/10.1039/d0ra09995c. PubMed PMID: 35423709; PubMed Central PMCID: PMCPMC8693363.

[90] A.J. Owoloye, F.C. Ligali, O.A. Enejoh, A.Z. Musa, O. Aina, E.T. Idowu, K.M. Oyebola, Molecular docking, simulation and binding free energy analysis of small molecules as PfHT1 inhibitors, Epub 20220826, PLoS One 17 (8) (2022) e0268269, https://doi.org/10.1371/journal.pone.0268269. PubMed PMID: 36026508; PubMed Central PMCID: PMCPMC9417013.

[91] N. Gan, Q. Sun, Z. Suo, S. Zhang, L. Zhao, H. Xiang, et al., How hydrophilic group affects drug–protein binding modes: differences in interaction between sirtuins inhibitors Tenovin-1/Tenovin-6 and human serum albumin, J. Pharmaceut. Biomed. Anal. 201 (2021) 114121, https://doi.org/10.1016/j.jpba.2021.114121.

[92] S. AlRawashdeh, K.H. Barakat, Applications of molecular dynamics simulations in drug discovery, Methods Mol. Biol. 2714 (2024) 127–141, https://doi.org/10.1007/978-1-0716-3441-7_7. PubMed PMID: 37676596.

[93] Meza M. Thuluz, J.-P. Claudia, C.Z. Rossana, Past, present, and future of molecular docking, in: G. Vishwanath, K. Partha, T. Ashit (Eds.), Drug Discovery and Development, IntechOpen, Rijeka, 2020. Ch. 2.

[94] A. Kakhar Umar, J.H. Zothantluanga, J.A. Luckanagul, P. Limpikirati, S. Sriwidodo, Structure-based computational screening of 470 natural quercetin derivatives for identification of SARS-CoV-2 M(pro) inhibitor, Epub 20230314, PeerJ 11 (2023) e14915, https://doi.org/10.7717/peerj.14915. PubMed PMID: 36935912; PubMed Central PMCID: PMCPMC10022500.

[95] S. Kundrapu, V.C. Sunkesula, L.A. Jury, J.L. Cadnum, M.M. Nerandzic, J.S. Musuuza, et al., Do piperacillin/tazobactam and other antibiotics with inhibitory activity against Clostridium difficile reduce the risk for acquisition of C. difficile colonization?, Epub 20160418, BMC Infect. Dis. 16 (2016) 159, https://doi.org/10.1186/s12879-016-1514-2. PubMed PMID: 27091232; PubMed Central PMCID: PMCPMC4835867.

[96] S.V. Pattar, S.A. Adhoni, C.M. Kamanavalli, S.S. Kumbar, In silico molecular docking studies and MM/GBSA analysis of coumarin-carbonodithioate hybrid derivatives divulge the anticancer potential against breast cancer, Beni-Suef University Journal of Basic and Applied Sciences 9 (1) (2020) 36, https://doi.org/10.1186/s43088-020-00059-7.

[97] X. Du, Y. Li, Y.L. Xia, S.M. Ai, J. Liang, P. Sang, et al., Insights into protein-ligand interactions: mechanisms, models, and methods, Epub 20160126, Int. J. Mol. Sci. 17 (2) (2016), https://doi.org/10.3390/ijms17020144. PubMed PMID: 26821017; PubMed Central PMCID: PMCPMC4783878.

[98] S.S. Jambhekar, Chapter 4 - equilibrium processes in pharmaceutics, in: A.K. Dash, S. Singh (Eds.), Pharmaceutics, second ed., Academic Press, 2024, pp. 115–143.